AIAA Paper
94-4381

Trim, Control and Landing Gear Effects in Variable-Complexity HSCT Design

P. E. MacMillin*, J. Dudley*, W. H. Mason,† B. Grossman,‡ and R. T. Haftka.§

Department of Aerospace and Ocean Engineering
and
Multidisciplinary Analysis and Design (MAD) Center for Advanced Vehicles
Virginia Polytechnic Institute and State University
Blacksburg, Virginia 24061

Abstract

Trim and control requirements have been added to our previous work developing multidisciplinary design methodology for the design of a high speed civil transport (HSCT). We are optimizing the design including both aerodynamics and structures to find the wing planform and thickness distribution, fuselage shape, and engine placement, using 28 design variables. While adding trim and control it was also found necessary to simultaneously consider landing gear integration. We include the engine out and cross wind landing requirements, as well as engine nacelle strike for lateral-directional requirements. We include nose-wheel lift-off rotation and approach trim as the critical conditions in the longitudinal plane. For lateral-directional requirements we found that the engine nacelle strike avoidance was the critical condition, although the vertical tail size was increased from the baseline design to account for the engine-out condition. The addition of a horizontal tail to provide take-off rotation resulted in a significant weight penalty, and the sensitivity to the placement of the landing gear axially was obtained by finding the minimum gross takeoff weight for two different tipback angles.

Introduction

The design of an efficient and economically feasible high-speed civil transport (HSCT) requires a multidisciplinary design approach. If any of the major disciplinary interactions are neglected in the conceptual/preliminary design phase, it is likely there will be a significant weight penalty in the final design because of the need to account for the neglected interactions after the configuration has been "frozen". At Virginia Tech, we are developing multidisciplinary design optimization (MDO) methodology to integrate the major disciplines in detail during the conceptual/preliminary design phase. Our specific HSCT design problem is to minimize the take-off gross weight of a Mach 2.4 configuration having a range of 5500*nm*.

The high cost of using detailed analysis methods in an MDO procedure prevents their use in conceptual design. To reduce the computational cost of MDO, we have been developing the variable-complexity modeling concept. Variable-complexity modeling uses multiple levels of analysis methods. For aerodynamics we use both detailed numerical methods, vortex lattice methods are used here to establish the methodology, and approximate analysis methods, which are generally analytical or empirically derived relations. Detailed numerical analysis methods are accurate but costly, so they are only used sparingly to improve the accuracy of the approximate analysis methods. The methodology allows the use of other, more advanced numerical methods. An in-depth discussion of the various types of variable-complexity approximations and the aerodynamic and structural analysis methods we are using can be found in the papers by Hutchison *et al.*[1-3]

In this paper we extend the previous work of Hutchison *et al.*[1-3] to include trim and control considerations directly in the variable-complexity design procedure. Our work uses the conceptual/preliminary design control authority assessment methods developed by Kay.[4] In particular, Kay established a set of stability and control requirements which must be addressed in the initial stages of vehicle design. An examination of the control requirements of HSCT configurations has recently been conducted by McCarty *et al* of McDonnell Douglas Aerospace.[5] Their work is consistent with the approach of Kay, and has been used to focus the work presented here. Based on references 4 and 5, we assume that the critical conditions for sizing control surfaces occur at low speed. The ratio of dynamic pressure at cruise (M2.4 at 65K ft) to the low speed critical field performance conditions (150kt, sea level) is more than 6.0. Thus, the high control power requirements during take-off and landing combined with the low dynamic pressure results in the low speed field performance conditions being the critical design conditions.

Making the assumption that the low speed cases define the control surface sizes, trim and control requirements are incorporated for both lateral-directional and longitudinal control surfaces. In the lateral directional case, the conditions are engine-out trim performance and cross-wind landing. For engine-out trim performance we require

---

* Graduate Research Assistant, Student Member AIAA
† Associate Professor, Assoc. Fellow AIAA
‡ Professor and Department Head, Assoc. Fellow AIAA
§ Christopher C. Kraft Professor, Assoc. Fellow AIAA
All in the Department of Aerospace and Engineering

the aircraft be capable of trimmed flight after one of the outboard engines fails. Essentially, the vertical tail must be capable of handling the yawing moment generated by the thrust imbalance. This is especially important because of the wing weight benefit of placing the engines as far outboard as posible. In the longitudinal axis, take-off rotation has been found to be the critical condition for this class of aircraft, and we consider take-off rotation and approach trim.

Explicit consideration of trim and control in conceptual aircraft sizing methodology is unusual. For subsonic configuration optimizations there have been two related studies. Sliwa[6,7] and Gallman *et al*[8] both considered longitudinal trim and control, and both found that the trim and control considerations were important. In the study by Gallman *et al*[8] the take-off rotation control requirement was found to be a critical issue in the comparison of equivalent conventional and joined-wing configurations.

As part of the integration of aircraft trim and control requirements, the engine and landing gear locations emerge as significant considerations. The engine location becomes important because of both asymmetric thrust considerations and the requirement that the engine nacelles not strike the runway during take-off and landing. Thus, the landing gear location and length play a key role in defining the control power required to rotate the aircraft at take-off. Both of these considerations are included in the methodology described in this paper.

Stability derivatives must be available to include trim and control in the optimization. We use our variable-complexity modeling concept to estimate them. This improves the accuracy without incurring high computer cost. Specifically, we use the so-called interlacing technique described by Dudley *et al.*[9] They used the approach to incorporate detailed finite element structural analysis in the optimization.

In the following sections we describe control surface and landing gear design issues. Then we mention the configuration issues, our baseline configuration and mission, and analysis methods. Then we discuss the results of a sensitivity analysis, compare a design optimized with vertical tail sizing, and a design optimized with horizontal tail sizing to a design optimized without any trim and control considerations.

Control Surface and Landing Gear Design Issues

To be viable, the aircraft must have sufficient control power for trimmed flight and still be able to perform required maneuvers such as take-off and landing, as well as in-flight maneuvers. If care is not taken in the early stages of design the resulting aircraft might not have the control power required, and late fixes may severely compromise the design. However, excessive control power can mean increased weight and drag, which will also reduce performance and increase operating costs.

Engine-Out Trim/Vertical Tail Sizing and Crosswind Landing

The engine-out condition is considered first. In civilian aircraft such as the HSCT, where maneuverability is not a primary consideration, vertical tail size is based either on the requirement that the aircraft be capable of trimmed flight with an outboard engine inoperative or to handle the crosswind landing requirement. The pilot must have sufficient control authority to trim the aircraft in these situations, as well as to be able to perform necessary maneuvers. Therefore, we require the aircraft be trimmed directionally using no more than 75% of the available control authority.

Deflecting the rudder creates the balancing yawing moment, but also causes a sideforce which must be counteracted. This is done with a combination of sideslip and bank. Both sideslip and bank can make landing difficult if the angle is too great. A large amount of sideslip will cause a very rough landing as the aircraft must suddenly straighten out upon touchdown. Excessive bank introduces the possibility of the wing tip scraping the ground before the landing gear touches down. These considerations require us to limit the allowable amount of sideslip and bank to 10° and 5°, respectively. The rudder deflection also creates a rolling moment that is usually controlled using the ailerons.

Engine Location Limits

Moving the engines outboard provides wing bending moment relief, thereby reducing the wing weight. Without any constraint the optimizer will position the engines off the wing tip to maximize this weight savings. Clearly, positioning the engines at the wing tip is unrealistic. This could cause problems with engine-out trim, engine strike during landing, airframe stresses during ground operations, such as full fuel taxi and flutter. A constraint is needed to prevent the optimizer from placing the engines too far outboard on the wing.

Landing Gear Position

Landing gear position is important for the center of gravity calculation, engine nacelle strike constraint, and take-off rotation. Both the nose and main gear positions must be known for the center of gravity calculation. On landing, the main gear touches down first, so the position and length of the main gear is critical to the engine and tail strike constraint. Increasing the length of the main gear results in more ground clearance, the distance between the nacelles and the runway. Moving the main landing gear closer to the engines on the wing reduces the effect of pitch and bank on the ground clearance. In general, pitch will reduce the ground clearance and bank will reduce ground clearance on the wing which is banked toward the ground and increase it on the other side.

The weight distribution on the landing gear is important during take-off rotation. If the nose gear is too heavily loaded, it will be difficult to rotate to the take-off

attitude. If the nose gear is too lightly loaded, the aircraft will be hard to steer and could rotate before there is enough control authority to control the aircraft's attitude. Other important considerations include the overturn angle and the tipback angle, (i.e., see Fig. 1 and 2). Both angles relate the main gear's position to the location of the center of gravity. If the main gear is not far enough behind the center of gravity, the aircraft could tip back and sit on its tail. If it is not far enough to the side of the *cg*, then the aircraft could tip over while taxiing around a sharp turn.

Take-off Rotation/Horizontal Tail Sizing and Approach Trim

Several longitudinal control and trim issues are important. The field performance requirements are among the most critical. For most airplanes, take-off involves rotating on the main landing gear to a pitch attitude at which the wings can generate enough lift to become airborne. This rotation is caused by the pitching moment generated by a longitudinal control effector such as the horizontal tail or the wing trailing edge flap for a tailless configuration. The civilian FAR[10] regulations essentially require the aircraft be able to take off safely. The military regulations, MIL-STD-1797[11], section 4.2.7.3, requires the aircraft to be able to obtain, at $0.9V_{min}$, a pitch attitude which will result in take-off at V_{min}, where V_{min} is 110% of the stall speed. This requires nose-wheel liftoff occur prior to $0.9V_{min}$, and then there must be enough pitch control to rotate the aircraft to the take-off attitude at $0.9V_{min}$.

Approach trim is also important. The aircraft must be able to trim at a high angle of attack, when the aerodynamic forces can be very large. There should be enough control power to trim and, if necessary, maneuver. This allows the pilot to deal with gusts and other emergency demands.

Typical Configuration and Mission

In this study of HSCT configurations, our basic configuration consists of a 300 ft. fuselage sized to carry 251 passengers, a cranked wing and a vertical tail (see Figure 3). The aircraft is powered by four low bypass turbofan engines. The mission we are designing our aircraft for is to transport 251 passengers, and their luggage, 5500 *nm*, with a cruise speed of Mach 2.4. The maximum altitude is 70,000 ft. and the aircraft must land with 15% of its fuel remaining. The field performance constraint is to be able to land at 12° angle of attack (AOA).

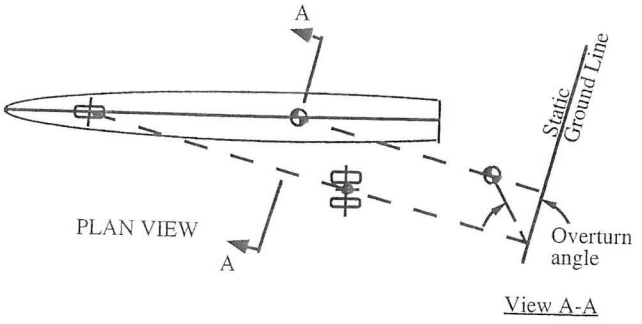

Figure 1. Definition of the overturn angle

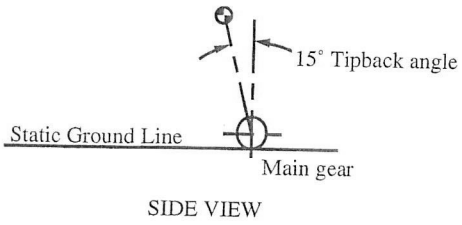

Figure 2. Definition of tipback angle

Using our analysis, the baseline configuration used to start the optimization process weighs 580,600 lbs, and has a range of 5,482 *nm*. It has a wing area of 12,141 ft^2 and a vertical tail area of 450 $ft.^2$ This design came from a previous optimization that did not include any trim and control considerations, but satisfies all other constraints.

Analysis Methods

To analyze trim and control conditions, it is necessary to obtain information not normally used in initial sizing programs. This includes the location of the center of gravity (*cg*), the inertias, and the stability and control derivatives. These are found for a given geometry and flight condition.

Center of Gravity and Inertia Estimation

In stability and control calculations the location of the center of gravity is very important, but estimation of the center of gravity in the preliminary design phase is not simple. During cruise and landing approach, we attempt to place the *cg* at the center of pressure by transferring fuel between tanks. This minimizes the use of control surfaces to trim the aircraft, reducing drag during the cruise. We can calculate the center of pressure for the wing at subsonic speed using a vortex lattice method (VLM) and, for this preliminary design, use this as the *cg*.

During take-off, it is not possible to place the *cg* at the center of pressure, and a more detailed estimation of the location of the *cg* must be used. We use estimates given by Roskam[12] to estimate the center of gravity of the various components, and place miscellaneous equipment, such as avionics and cargo, using an initial estimate of the aircraft layout. The fuselage *cg* is placed at 45% of the length. The wing *cg* is placed at 55% of the wing chord at 35% of the semispan. The horizontal tail *cg* is placed at 42% of the chord from the leading edge, at 38% of the semispan. The vertical tail *cg* is placed using the same formula as the horizontal tail. Finally, the engine *cg* is placed at 40% of the nacelle length. Once the *cg* for each of the components is calculated, it is straightforward to calculate the *cg* for the aircraft. The inertias for the aircraft are esti-

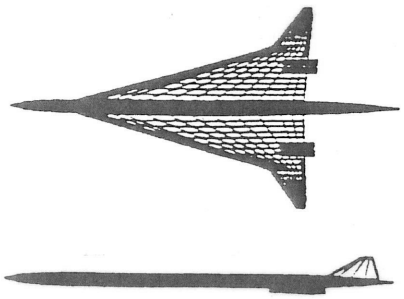

Figure 3. Typical configuration

mated using a routine from FLOPS[13] which is based on a modified DATCOM[14] method.

Stability Derivative Estimation

The analysis of the take-off rotation and engine out condition requires stability derivatives. We have two methods of calculating stability derivatives, empirical algebraic relations from the U.S.A.F. Stability and Control DATCOM[14], as interpreted by J. Roskam,[15] and a VLM code developed by Kay.[4] The DATCOM methods rely on simple theories and some experimental data, and do not handle unusual configurations well. A detailed discussion of the approximate methods we use is given in Appendix A. The VLM code is better able to handle different configurations, but is more expensive computationally.

To achieve reasonable accuracy and computational cost, we used both methods in a variable-complexity analysis approach. We estimate the derivatives with the VLM code every five optimization cycles, and use the DATCOM estimates to scale the derivatives in between the VLM calculations. The VLM code makes the initial prediction of the stability derivatives, and then the DATCOM methods are used to predict the trends as the configuration geometry is changed during the optimization. This approach is similar to the variable-complexity approach termed *interlacing*, used by Dudley *et al.*[9]

Accuracy of Stability Derivative Estimates

To test the accuracy of the DATCOM and VLM based predictions, we compared the results from both methods with experimentally determined stability and control derivatives. We modeled an XB-70A, in the powered approach configuration, using data from Heffley.[16] Since the vertical tail is the primary factor in this calculation, only the vertical tail contribution is calculated for the β derivatives. Similarly, the effect of the aileron derivatives is considered small, so these are not calculated with the DATCOM methods, but are updated with the VLM estimates.

Table 1

Comparison of stability and control derivative estimations

Derivative	Experiment	VLM	DATCOM
$C_{y\beta}$	-0.183	-0.177	-0.088
$C_{l\beta}$	-0.072	-0.011	0.0016
$C_{n\beta}$	0.132	0.042	0.036
$C_{y\delta r}$	0.120	0.152	0.072
$C_{l\delta r}$	-0.0018	0.0035	-0.0013
$C_{n\delta r}$	-0.103	-0.077	-0.029
$C_{y\delta a}$	-0.063	0.0	0.0
$C_{l\delta a}$	0.042	-0.095	-------
$C_{n\delta a}$	-0.0052	0.0086	-------

Table 2

Comparison of stability derivatives for a F/A-18[4] at Mach 0.2, out of ground effect

Derivative	Experiment	VLM	DATCOM
$C_{y\beta}$	-0.917	-0.526	-0.561
$C_{l\beta}$	-0.050	-0.080	-0.055
$C_{n\beta}$	0.096	0.086	0.066
$C_{y\delta r}$	0.134	0.108	0.103
$C_{l\delta r}$	0.012	0.017	0.015
$C_{n\delta r}$	-0.046	-0.045	-0.030
$C_{l\delta a}$	0.150	0.167	0.136

Table 1 compares the experimental results with the VLM and DATCOM approximations. Generally, the VLM results are good, although there are sign discrepancies on $C_{l\delta r}$, and $C_{n\delta a}$. This is most likely due to poor modeling of the XB-70A in Kay's VLM code, which defines the planform and the side view with 5 trapezoids for each. A code which allowed more detailed models could improve these results. The DATCOM results also have a sign discrepancy, on $C_{l\beta}$, but this term is only the tail contribution, not the derivative for the entire aircraft.

Comparison of experimental, VLM, and DATCOM results for a F/A-18 from Kay shows good agreement between the experimental and the VLM data, notably the $C_{n\beta}$ and $C_{n\delta r}$ derivatives. Some of his results[4] are shown in Table 2.

Landing Gear Analysis

As a first approximation, the main gear was placed at 80% of the wing root chord. This was adequate for the engine strike constraint, and was used for the optimizations that did not include the take-off rotation requirement. The nose gear location was not required at that time.

To analyze the take-off rotation, the nose gear position was needed. Torenbeek[17] recommends the nose gear support between 8% and 15% of the total weight. We elected to place the nose gear so that it would be supporting 11.5% of the total weight. As initially positioned, we discovered that the main gear was too far back, the nose gear was supporting over 22% of the weight, and could not be located on the aircraft and support 11.5% of the weight. So it was necessary to move the main gear for-

ward from 80% of the wing root chord.

From the calculated *cg* location, we calculate the tipback angle. This is the angle between the main gear and the *cg* as seen in the side view and it should be about 15°. By specifying this angle, the position of the main gear can be calculated. We found that a tipback angle of 15° resulted in a reasonable position for both the main gear and the nose gear. After the landing gear was positioned, the overturn angle was calculated. This is a measure of the likelihood of the aircraft tipping over sideways while taxiing in a turn. It should be less than 63°. This was not a critical consideration for our design.

Engine Strike

We originally expected the engine out condition would limit the allowable spanwise engine location since as the engines move outboard, the vertical tail size must be increased. We thought the increase in vertical tail weight and additional drag on the larger tail would offset the savings in wing weight. As shown below, we were wrong. As the engine moves outboard, the increase in vertical tail weight is very small compared to the reduction in wing weight, this can be seen in Fig. 4. The increase in vertical tail weight is 4,000 lbs, but the decrease in wing weight is over 20,000 lbs. Also, the increase in wave drag due to increasing vertical tail size is small, as can be seen in Fig. 5. The increase is less than two counts, at most. Thus the minimum TOGW is achieved by having a very large vertical tail and placing the engines as far outboard as possible. This was confirmed when the optimizer placed the engines off the wing tip.

Thus, another consideration was needed to constrain the spanwise engine location. The engine strike constraint requires that the engines do not strike the runway during landing. We calculate the engine height at touchdown with the pitch angle equal to the landing angle of attack and the bank angle equal to 5°, the typical certification requirement. This constraint not only limits the spanwise engine location, but effectively limits the allowable trailing edge sweep, because the engines are mounted at the trailing edge, with 25% overhang.

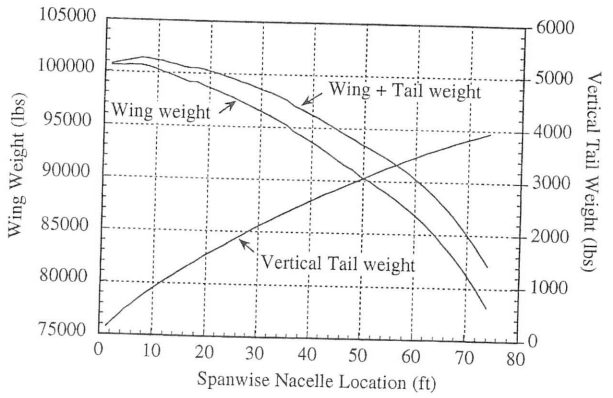

Figure 4. The sum of wing and vertical tail weights decreases as the engine is moved outboard.

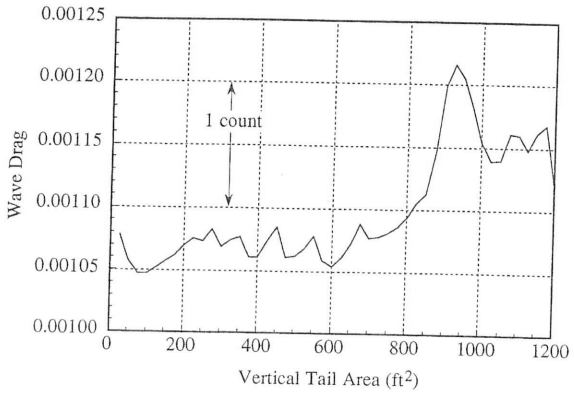

Figure 5. The wave drag increases very little with nacelles moving outboard and increasing in vertical tail area.

Vertical Tail Analysis

As a first step in integrating the design of the vertical tail with the design of the rest of the aircraft, we added a single design variable for the vertical tail area. We maintain the shape of the vertical tail, specifying the aspect ratio, taper ratio, and quarter chord sweep, and vary its size. After finding the stability derivatives for a given tail size, we calculate the control surface deflections and engine location required for trimmed flight. In trimmed flight the sum of the forces and moments must be zero. This can be expressed with the following equations:

Sideforce:

$$C_{y_{\delta a}}\delta_a + C_{y_{\delta r}}\delta_r + C_{y_\beta}\beta + C_L \sin\phi = -\frac{Y_{ext}}{qSb} \tag{1}$$

Rolling moment:

$$C_{\ell_{\delta a}}\delta_a + C_{\ell_{\delta r}}\delta_r + C_{\ell_\beta}\beta = -\frac{L_{ext}}{qSb} \tag{2}$$

Yawing moment:

$$C_{n_{\delta a}}\delta_a + C_{n_{\delta r}}\delta_r + C_{n_\beta}\beta = -\frac{N_{ext}}{qSb} \tag{3}$$

The net yawing moment due to engine failure is $N_{ext} = y_{eng}\Delta T$, where y_{eng} is the y distance from the fuselage centerline to the engine, and ΔT is the thrust difference due to the engine loss (with engine loss on the right wing corresponding to positive ΔT). By assuming that the net rolling moment, L_{ext}, and the net side force, Y_{ext}, are zero, equations (1) - (3) can be solved for bank angle, ϕ, aileron deflection, δ_a, and engine location, y_{eng}.

$$\phi = \sin^{-1}\left(\frac{\delta_r\left(\frac{C_{y_{\delta a}}C_{\ell_{\delta r}}}{C_{\ell_{\delta a}}} - C_{y_{\delta r}}\right) - \beta\left(C_{y_\beta} - \frac{C_{y_{\delta a}}C_{\ell_\beta}}{C_{\ell_{\delta a}}}\right)}{C_L}\right) \tag{4}$$

$$\delta_a = -\frac{C_{\ell_{\delta r}}\delta_r + C_{\ell_\beta}\beta}{C_{\ell_{\delta a}}} \tag{5}$$

$$y_{eng} = -\frac{qSb}{\Delta T}\left(C_{n_{\delta a}}\delta_a + C_{n_{\delta r}}\delta_r + C_{n_\beta}\beta\right) \tag{6}$$

The bank angle is determined by minimizing β, without violating the 5° limit imposed on ϕ. Equation (5) can be solved by setting the rudder deflection to 75% of the maximum allowable deflection. Then it is possible to solve equation (6) for the maximum outboard location of the engine.

Crosswind Landing

We required the aircraft be able to land with a 20 knot crosswind. Since our approach speed is 145 knots, this results in a sideslip angle of 7.85°. The aircraft must be able to trim directionally at a sideslip of 7.85°. Using equations (1) through (3), where β is known, and all right hand side terms are zero, it is possible to solve for bank angle, ϕ, aileron deflection, δ_a, and the rudder deflection, δ_r. This results in

$$\delta_r = \frac{\left(\frac{C_{n_{\delta a}}C_{\ell_\beta}}{C_{\ell_{\delta a}}} - C_{n_\beta}\right)}{\left(C_{n_{\delta r}} - \frac{C_{n_{\delta a}}C_{\ell_{\delta r}}}{C_{\ell_{\delta a}}}\right)}\beta \tag{7}$$

$$\delta_a = -\frac{C_{\ell_{\delta r}}\delta_r + C_{\ell_\beta}\beta}{C_{\ell_{\delta a}}} \tag{8}$$

$$\phi = \sin^{-1}\left[-\frac{1}{C_L}\left(C_{y_{\delta a}}\delta_a + C_{y_{\delta r}}\delta_r + C_{y_\beta}\beta\right)\right] \tag{9}$$

We added constraints to limit the rudder and aileron deflections to 22.5°, 75% of their assumed maximum deflections, and the bank angle to 5°. For our HSCT work this constraint was not found to be critical. The engine-out constraint was critical for our designs.

Horizontal Tail Analysis

Another design variable was added for the horizontal tail. Like the vertical tail, we maintain the shape of the horizontal tail with only the size changing. The analysis of the horizontal tail consists of two parts. First, the rotation speed must be calculated, then it must be shown that the aircraft can rotate to the take-off attitude, at $0.9V_{min}$. V_{min} is calculated from

$$V_{\min} = 1.1\sqrt{\frac{2W}{\rho S C_{L_{\alpha\max}}}} \tag{10}$$

where the density, ρ, is assumed to be sea level standard, and $C_{L_{\alpha max}}$ is assumed to be 0.9, which is based on a limit on angle of attack.

The minimum rotation speed for the configuration is calculated by setting the sum of the forces and moments equal to zero. Taking the moment about the *cg* and assuming there is no reaction force at the nose wheel allows the equations to be solved for the dynamic pressure necessary to start rotating the aircraft, from which the minimum rotation speed can be found. We require the minimum rotation speed to be less than $0.9V_{min}$.

The moment about the *cg* at nosewheel liftoff is given by

$$M_{cg} = Tz_T + qSC_D z_D - qSC_L x_L + F_{mg}\left(z_{mg}\sin\alpha - x_{mg}\cos\alpha\right) - \mu F_{mg}\left(z_{mg}\cos\alpha + x_{mg}\sin\alpha\right) + qS\bar{c}C_M \tag{11}$$

where T is the thrust, z_T is the vertical distance between the thrust vector and the *cg*, z_D is the vertical distance between the aerodynamic center and the *cg*, x_L is the horizontal distance between the aerodynamic center and the *cg*, F_{mg} is the reaction force on the main wheels, given by

$$F_{mg} = \frac{W - qSC_L}{\cos\alpha + \mu\sin\alpha} \tag{12}$$

Also, x_{mg} and z_{mg} are the horizontal and vertical distances between the point where the main gear touches the runway and the *cg*, and μ is the friction coefficient for the runway, assumed to be 0.02. The angle of attack, α, is zero for the rotation velocity calculation.

The net moment at nosewheel liftoff is zero. This allows equation (11) to be solved for the rotation dynamic pressure, q_r, which gives the rotation speed, V_r.

$$q_r = \frac{W\left(x_{mg} + mz_{mg}\right) - Tz_T}{S\left(C_D z_D + C_L\left(x_{mg} - x_L + mz_{mg}\right) + \bar{c}C_M\right)} \tag{13}$$

$$m = \frac{\mu\cos\alpha - \sin\alpha}{\cos\alpha + \mu\sin\alpha} \tag{14}$$

$$V_r = \sqrt{\frac{2q_r}{\rho}} \tag{15}$$

If the aircraft has a minimum rotation speed which does not exceed $0.9V_{min}$, the second requirement is to insure there is adequate control power to rotate the aircraft to the proper pitch attitude at a speed of $0.9V_{min}$. This can be done by numerically intergrating

$$M_{cg} = I_{yy_{cg}}\ddot{\alpha} \tag{16}$$

which simulates the rotation process, where M_{cg} is calculated from equation (11). This involves calculating the moment about the *cg* and numerically integrating to solve for α. This is iterated until the aircraft has reached take-off attitude, or the speed exceeds $0.9V_{min}$. If the aircraft does not reach the take-off attitude, then a larger horizontal tail is needed.

To calculate the aerodynamic coefficients for the

horizontal tail, it is necessary to calculate the downwash angle, ε. This angle can be approximated using

$$\varepsilon = \varepsilon_0 + \frac{d\varepsilon}{d\alpha}\alpha \tag{17}$$

and ε_0 can be neglected. The change in downwash with respect to angle of attack can be calculated using the following equations:

$$\frac{d\varepsilon}{d\alpha} = 4.44\left[K_A K_\lambda K_H \left(\cos\Lambda_{c/4}\right)^{1/2}\right]^{1.19} \tag{18}$$

$$K_A = \frac{1}{AR} - \frac{1}{1+AR^{1.7}} \tag{19}$$

$$K_\lambda = \frac{10-3\lambda}{7} \tag{20}$$

$$K_H = \frac{1-\frac{h_H}{b}}{\left(\frac{2l_H}{b}\right)^{1/3}} \tag{21}$$

Powered Approach Trim

The powered approach trim constraint requires the aircraft to have sufficient control authority for longitudinal trim during the approach. The aircraft approaches at a landing speed of 145 knots and is at the landing angle of attack, which is constrained to be less than 12°.

Like the take-off requirements, this constraint involves calculating the pitching moment about the *cg*, but in this case the net pitching moment should be zero. This is given by

$$M_{cg} = Tz_T + qSC_D z_D - qSC_L x_L + qS\bar{c}C_M = 0 \tag{22}$$

which can be rewritten as

$$C_M = \frac{1}{\bar{c}}\left(C_L x_L - C_D\left(z_T + z_D\right) - \frac{W\sin\alpha}{qS} z_T\right) \tag{23}$$

This is the pitching moment generated by the lift, drag, thrust, and weight. The pitching moment to balance this is given by

$$C_M = C_{M_\alpha}\alpha + C_{M_0} \tag{24}$$

or

$$C_M = C_{M_\alpha}\alpha + C_{L_{\alpha t}} V_H i_t\left[1 - \frac{C_{L_{\alpha t}} S_t}{C_{L_\alpha} S}\left(1 - \frac{d\varepsilon}{d\alpha}\right)\right] \tag{25}$$

This can be solved for the horizontal tail deflection, i_t,

$$i_t = \frac{C_M - C_{M_\alpha}\alpha}{C_{L_{\alpha t}} V_H\left[1 - \frac{C_{L_{\alpha t}} S_t}{C_{L_\alpha} S}\left(1 - \frac{d\varepsilon}{d\alpha}\right)\right]} \tag{26}$$

Substituting the pitching moment calculated in equation (23) into this gives the required tail deflection. The tail deflection was limited to 22.5°. This was not an active constraint.

The Optimization Method

Since an optimization using only exact analysis methods would be very expensive computationally, we perform sequential approximate optimization. At the start of each optimization cycle, approximations are set up using a combination of simplified and exact methods. Then we place move limits on the design variables, to stay within a valid region of the approximations, and the optimizer is allowed to converge. This is repeated until the exact analysis of the design converges.

We use the NEWSUMT-A program[18] to perform the approximate optimization. NEWSUMT-A uses a sequential unconstrained minimization technique with an extended interior penalty function. It uses Newton's method with approximate second derivatives, for unconstrained minimization.

Numerical optimization of an aircraft configuration requires both the configuration and the mission parameters to be described with a set of design variables. Prior to the addition of the current trim and control considerations, there was a total of twenty six design variables. The idealized cruise mission is defined by three variables: mission fuel, initial altitude, and constant climb rate (with altitude held constant if it reaches 70K ft.). Eight design variables are used to describe the wing planform, and five more are used to define the airfoil thickness distribution. The engine nacelles are placed along the trailing edge, with 25% overhang. Two variables are used to indicate the spanwise location of the nacelles. The axisymmetric fuselage is defined using eight design variables. These twenty three design variables define the aircraft parameters. The analysis is done using a Craidon format geometry file[19] to completely describe the configuration. The use of this format allows an analysis to be made using detailed computational methods. To include trim and control considerations the horizontal and vertical tail areas were added as design variables.

Our objective is to minimize take-off gross weight while satisfying sixty five constraints, including a range of 5500 *nm* at Mach 2.4, with 251 passengers. Because we use approximate analysis during the optimization, the range generally is not 5500 *nm*. We adjust the GTOW for a range deficiency or surplus by taking the difference between our goal of 5500 *nm* and the calculated range and multiplying by a factor of 90. This is then added to the GTOW, to get the corrected GTOW. This accounts for the deficiency or surplus in fuel. Other constraints include performance, aerodynamic, and geometric constraints, such as a minimum wing chord and landing tail scrape angle. These prevent the optimizer from creating physically impossible designs. In this work we have added constraints which require that the outboard engine nacelle not strike the runway, the vertical tail be large enough to trim the aircraft with one engine inoperative, and that the aircraft

achieves take-off pitch attitude at $0.9V_{min}$.

Prior to the addition of the vertical and horizontal tail considerations, the nacelles were constrained to be within 50% of the wing semi-span. The addition of the vertical tail sizing changes the nacelle constraint to be within the limit imposed by the vertical tail or the engine strike constraint. This insures the aircraft could safely handle an engine-out situation. Adding the horizontal tail consideration adds two constraints. The minimum rotation speed must be less than $0.9V_{min}$. Also, the velocity at which the aircraft attains the proper take-off pitch attitude must be less than or equal to $0.9V_{min}$.

Results

Sensitivity Analysis

First, we performed a sensitivity analysis to understand which design considerations contribute to the tail size. Each of the variables in the calculation of the limit on engine location was varied by 1%. Then we calculated the percent change in the limit on engine location which is the logarithmic derivative of the limit, denoted in Table 3 as the "sensitivity". This analysis showed the vertical tail placement, center of gravity location, and vertical tail area to be the most important variables for this calculation. The analysis also showed the engine location to be most sensitive to the yawing moment derivatives, especially the derivative of the coefficient of yawing moment with respect to sideslip, .

The sensitivities to the position of the vertical tail quarter chord and *cg* are somewhat misleading, in that one percent of the distance from the nose to the vertical tail quarter chord is 2.56 *ft.* and one percent of the distance from the nose to the *cg* is 1.6 *ft.* A one foot change in either will result in the same change in the engine location. The two parameters have the same sensitivity when calculated per foot, the difference here is due to the magnitude of the parameters.

Design Optimized with Vertical Tail Considerations

We performed an optimization, adding the engine-out consideration and the engine strike constraint, with the landing pitch angle equal to the landing angle of attack. Both of these constraints were violated by the baseline design. Even with the landing gear at 80% of the wing root chord, the nacelles would still be buried in the runway at landing and if an engine stalled, the aircraft would go into a spin.

The results of this optimization, case 1, has a gross take-off weight of 589,400 *lbs*, a wing area of 12,456 ft^2, and an aspect ratio of 2.05. The vertical tail area has increased to 548 $ft.^2$, from 450 $ft.^2$, while the outboard engine moved in to 27.7 ft. from the fuselage center line, or 34.5% of the semispan. Case 1 is shown in Fig. 6. Table 4 compares the weight breakdowns and major design variables of the baseline design and case 1.

The primary change is in the vertical tail size and

Table 3 Logarithmic sensitivity of engine location limit to selected parameters

Parameter	Sensitivity
Distance from nose to vertical tail quarter chord	2.545
Distance from nose to center of gravity	-1.587
Vertical tail area	1.106
Rudder deflection	0.705
Sideslip angle	0.296
Wing area	-0.025
$C_{y\beta}$	0.0
$C_{l\beta}$	0.002
$C_{n\beta}$	0.294
$C_{y\delta r}$	0.0
$C_{l\delta r}$	0.019
$C_{n\delta r}$	0.686
$C_{y\delta a}$	0.0
$C_{l\delta a}$	-0.020
$C_{n\delta a}$	0.021

spanwise engine locations. The vertical tail area increased 22% from the baseline. This is a direct result of the engine out consideration, the vertical tail had to be larger for the engine location. The engines moved inboard to satisfy the engine strike constraint. Another effect of the engine strike constraint is the reduction in sweep of the inboard trailing edge. This allows the engines to move outboard, improving the structural design, but degrading the aerodynamic design. The maximum lift to drag ratio is reduced by about 1%, causing an increase in the required fuel weight. Increasing the vertical tail size increased the weight of the vertical tail by almost 19%, but the vertical tail weight is still less than 0.5% of the total weight. Moving the engines in caused the wing weight to increase by over one thousand pounds. Although it is heavier than the baseline design, which did not meet the requirements, this results in a good design.

The approximate stability derivative predictions in this case were in reasonable agreement with the VLM predictions. There is a jump that occurs every five cycles, this is the difference between the approximate and the VLM

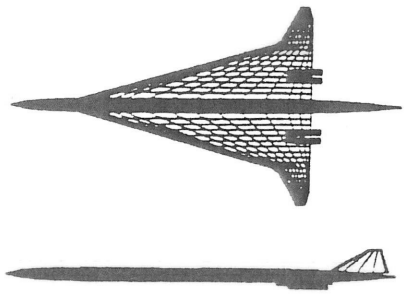

Figure 6. Case 1, final design

Table 4

Comparison of Baseline Design and Case 1

	Baseline	Case 1	% change
Gross Weight (*lbs*)	580,600	589,400	1.51
Fuel Weight (*lbs*)	280,300	287,000	2.40
Fuel / Gross	48.3%	48.7%	0.08
Wing Area (ft^2)	12,141	12,456	2.59
Wing Weight (*lbs*)	97,300	98,600	1.36
Vert. Tail Area (ft^2)	450.0	548.4	21.87
Vert. Tail Wght (*lbs*)	1,700	2,100	18.80
Aspect Ratio	2.12	2.05	-3.30
LE Sweep: inboard	74.18°	73.78°	-0.54
outboard	35.93°	29.02°	-19.23
TE Sweep: inboard	3.71°	0.27°	-92.72
outboard	-10.32°	-16.46°	-59.50
Nacelle 2 loc., y (*ft*)	36.3	27.7	-23.69
Range (*nm*)	5,481.9	5,497.5	0.28
Landing Angle (°)	11.96	11.97	0.08
$(L/D)_{max}$	9.988	9.893	-0.95

predictions. The history of $C_{y\delta r}$, $C_{l\delta r}$,$C_{n\delta r}$ and throughout the optimization process is shown in Figures 7a, b, and c. The approximate methods worked well, even in the first five cycles, where there was a large increase in the vertical tail size.

We performed a second optimization which also included the engine-out consideration and the engine strike constraint, but in this case the landing pitch angle is set to the landing angle of attack minus 3°. Reducing the landing pitch angle simulates a possible effect of high lift devices. This optimized design, case 2, has a gross take-off weight of 573,800 lbs., wing area of 11997 ft.^{2}, and an aspect ratio of 2.13. Case 2 is shown in Figure 8. Table 5 compares the weight breakdowns and major design variables of the

Table 5

Comparison of Baseline Design and Case 2

	Baseline	Case 2	% change
Gross Weight (*lbs*)	580,600	573,800	-1.18
Fuel Weight (*lbs*)	280,300	281,600	0.44
Fuel / Gross	48.3%	49.1%	1.66
Wing Area (ft^2)	12,141	11,997	-1.19
Wing Weight (*lbs*)	97,300	87,500	-10.07
Vert. Tail Area (ft^2)	450.0	1,017.4	126.1
Vert. Tail Wght (*lbs*)	1,700	3,400	99.31
Aspect Ratio	2.12	2.13	0.47
LE Sweep: inboard	74.18°	74.05°	-0.18
outboard	35.93°	28.44°	-20.85
TE Sweep: inboard	3.71°	0.24°	-93.53
outboard	-10.32°	-15.43°	-49.52
Nacelle 2 loc., y (*ft*)	36.3	58.5	61.16
Range (*nm*)	5,481.9	5,496.7	0.27
Landing Angle (°)	11.96	11.90	-0.50
$(L/D)_{max}$	9.988	9.807	-1.81

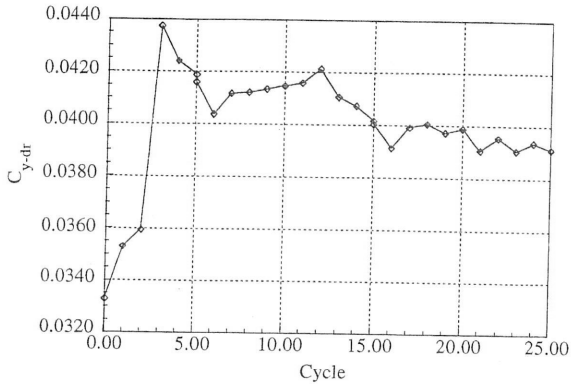

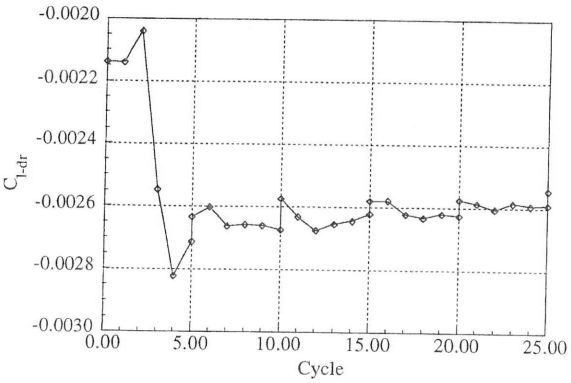

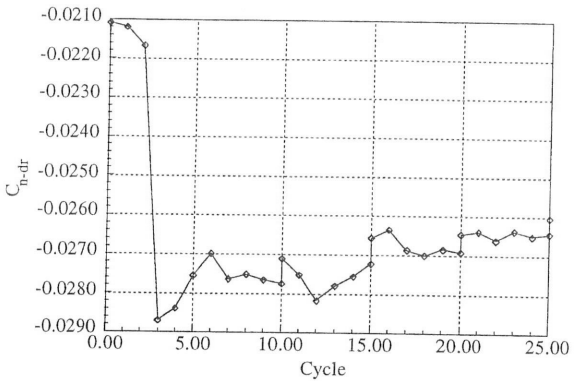

Figure 7. History of stability derivatves for Case 1

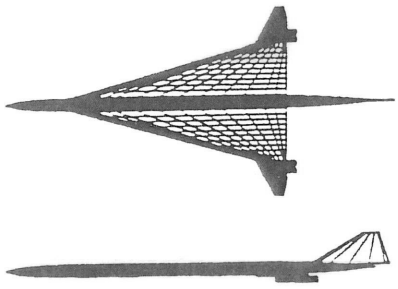

Figure 8. Case 2, final design

baseline design and case 2.

The vertical tail area increased dramatically to 1,017 ft.^{2}, while the outboard engine moved out to 58.5 ft. from the fuselage centerline. Reducing the landing pitch angle relaxed the engine strike constraint, allowing the engines to move outboard. This reduces wing weight, but requires a larger vertical tail. As was mentioned before, the increase in vertical tail weight does not offset the wing weight savings. Again, the trailing edge is practically unswept, as in case 1. This reduces the maximum lift to drag ratio by 1.81%, reducing the aerodynamic efficiency. So, despite the structural weight reduction, the fuel weight must increase to compensate for the reduction in lift to drag ratio.

Design Optimized with Vertical and Horizontal Tail Considerations

We performed three optimizations of designs using both the vertical and horizontal tail considerations. The first two, cases 3 and 4, were started from the same baseline design as cases 1 and 2, with the addition of a horizontal tail. This design is shown in Figure 9. Adding the horizontal tail to the baseline design caused the range to decrease from 5481.9 n.mi. to 5116.5 n.mi. and the maximum L/D to decrease from 9.988 to 9.599. The GTOW increased almost 12,000 lbs and the corrected GTOW increased by 44,575 lbs. Adding a horizontal tail increases the baseline weight a relatively small amount, about 2%, but causes a large decrease in range, which requires considerable additional fuel to meet the range requirement.

In case 3, the tipback angle was set to 30°. After 25 cycles of optimization, the aircraft had a gross take-off weight of 711,700 lbs. Case 3 is compared to the baseline in Table 6, and is shown in Figure 10. Clearly, the horizontal tail is too large. This is due to the excessively large tipback angle requirement. The table shows an increase in weight of almost 120,000 lbs, 90,000 lbs of this increase is for fuel. This can be explained by the decrease in maximum L/D, which is caused by the drag increase due to the larger vertical and horizontal tails.

In case 4, the tipback angle was reduced to 15°. This moved the main gear forward just over six feet on the baseline design. The two initial conditions were the same otherwise. Although a change of six feet seems small, the distance between the *cg* and the main gear was reduced by about 54%. This reduction in moment arm meant a smaller horizontal tail could be used to rotate the aircraft at take-off.

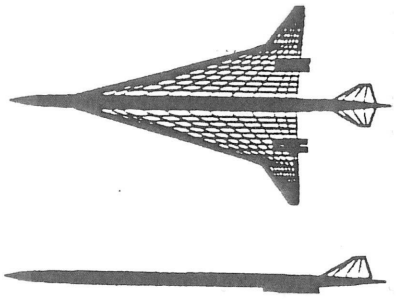

Figure 9. Baseline with horizontal tail

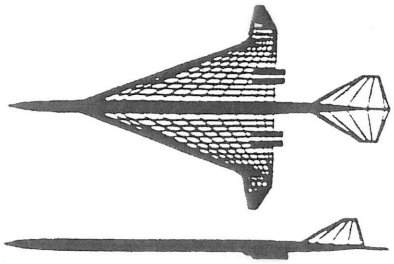

Figure 10. Case 3, final design

Table 6

Comparison of Baseline Design and Case 3

	Baseline	Case 3	% change
Gross Weight (*lbs*)	592,300	711,700	20.17
Fuel Weight (*lbs*)	280,300	370,200	32.06
Fuel / Gross	48.3%	52.0%	7.66
Wing Area (ft^2)	12,141	12,986	6.96
Wing Weight (*lbs*)	98,200	115,900	18.00
Vert. Tail Area (ft^2)	450.0	742.4	64.98
Vert. Tail Wt (*lbs*)	1,700	2,800	61.70
Horz. Tail Area (ft^2)	1,500.0	2,537.4	69.16
Horz. Tail Wt (*lbs*)	7,900	13,900	75.49
Aspect Ratio	2.12	2.41	13.68
LE Sweep: inboard	74.18°	69.39°	-6.46
outboard	35.93°	12.31°	-65.74
TE Sweep: inboard	3.71°	0.49°	-86.79
outboard	-10.32°	-32.02°	-210.27
Nacelle 2 loc., y (*ft*)	36.3	31.3	-13.77
Range (*nm*)	5,116.5	5,447.9	6.48
Landing Angle (°)	11.95	11.86	-0.75
$(L/D)_{max}$	9.599	9.807	-5.95

In this case, our best design had a gross take-off weight of 648,500 lbs. Case 4 is compared to the baseline in Table 7, and is shown in Figure 11. As in case 3, 75% of the weight increase is fuel weight. Unlike case 3 though, the horizontal tail area actually decreases from the baseline size. Moving the main gear by just six feet allowed the weight to decrease by over 60,000 lbs.

The stability derivative predictions in this case were excellent. There is almost no difference between the approximate and the VLM predictions. A history of $C_{y\delta r}$, $C_{l\delta r}$, and $C_{n\delta r}$ throughout the optimization process is shown in Figures 12a, b, and c. This method of stability derivative prediction is very effective. It provides reasonable accuracy at very little computer cost.

Case 5 was started from a different initial design, which is shown in Figure 13. This case converged to a local minimum which is considerably heavier than case 4

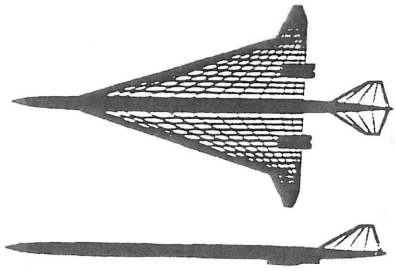

Figure 11. Case 4, final design

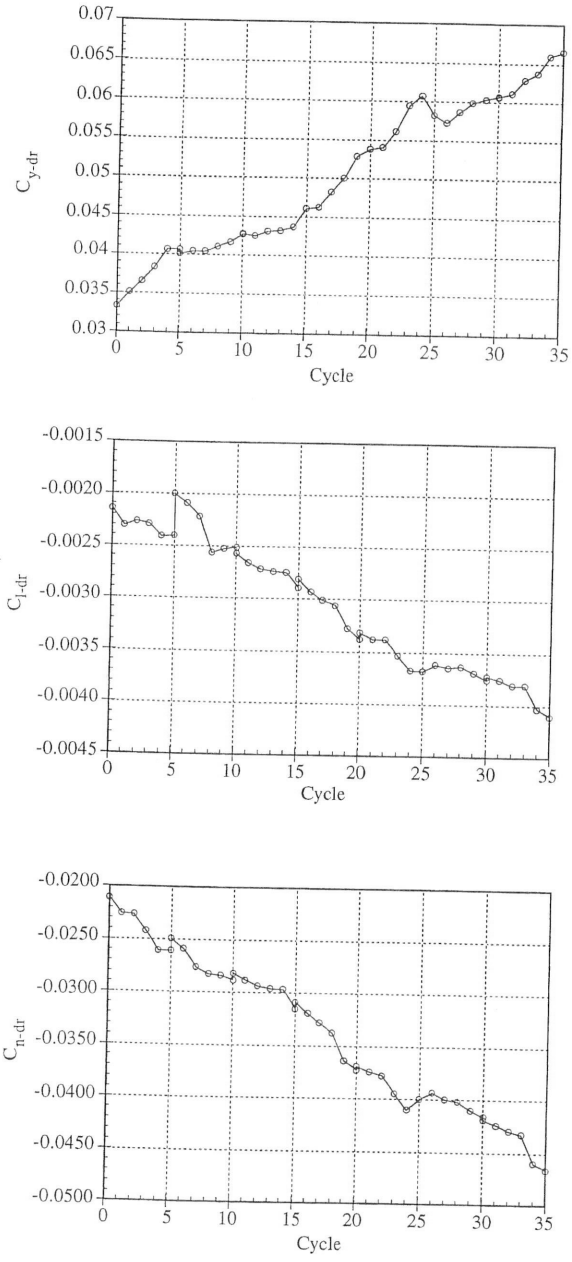

Figure 12. History of stability derivatves for Case 4

Table 7

Comparison of Baseline Design and Case 4

	Baseline	Case 4	% change
Gross Weight (*lbs*)	592,300	648,500	9.49
Fuel Weight (*lbs*)	280,300	322,600	15.09
Fuel / Gross	48.3%	49.8%	3.11
Wing Area (ft^2)	12,141	13,437	10.67
Wing Weight (*lbs*)	98,200	118,900	21.06
Vert. Tail Area (ft^2)	450.0	697.9	55.09
Vert. Tail Wt (*lbs*)	1,700	2,600	49.22
Horz. Tail Area (ft^2)	1,500.0	1,426.1	-4.93
Horz. Tail Wt (*lbs*)	7,900	7,700	-3.19
Aspect Ratio	2.12	2.00	-5.66
LE Sweep: inboard	74.18°	72.47°	-2.31
outboard	35.93°	27.13°	-24.49
TE Sweep: inboard	3.71°	0.11°	-97.04
outboard	-10.32°	-23.31°	-125.87
Nacelle 2 loc., y (*ft*)	36.3	32.4	-10.74
Range (*nm*)	5,116.5	5,511.7	7.72
Landing Angle (°)	11.95	11.97	0.17
$(L/D)_{max}$	9.599	9.663	0.67

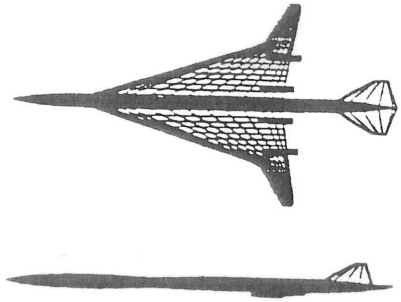

Figure 13. Case 5, initial design

Table 8

Comparison of Starting and Ending Designs for Case 5

	Initial	Final	% change
Gross Weight (*lbs*)	639,200	696,600	8.99
Fuel Weight (*lbs*)	320,100	363,200	13.44
Fuel / Gross	50.1%	52.1%	3.99
Wing Area (ft^2)	12,585	13,311	5.76
Wing Weight (*lbs*)	102,900	112,900	9.72
Vert. Tail Area (ft^2)	450.0	716.3	59.18
Vert. Tail Wt (*lbs*)	1,800	2,700	52.39
Horz. Tail Area (ft^2)	1,500.0	1,767.4	17.83
Horz. Tail Wt (*lbs*)	8,100	9,700	19.86
Aspect Ratio	2.22	2.22	0.00
LE Sweep: inboard	71.98°	69.47°	-3.49
outboard	31.56°	34.02°	7.79
TE Sweep: inboard	9.94°	0.96°	-90.34
outboard	-17.22°	-15.66°	9.06
Nacelle 2 loc., y (*ft*)	38.8	34.2	-11.86
Range (*nm*)	5,284.6	5,508.9	4.24
Landing Angle (°)	12.89	12.00	-6.90
$(L/D)_{max}$	9.602	9.314	-3.00

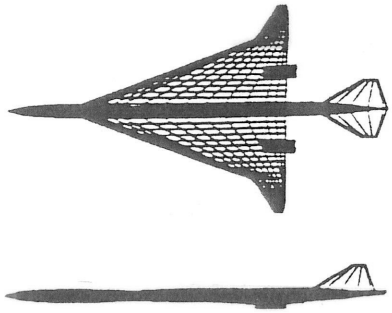

Figure 14. Case 5, final design

and is compared to the initial design in Table 8. The case 5 final design is shown in Figure 14, and although this design looks very similar to the case 4 design, the case 5 design has a lower maximum L/D. This increases the fuel required to complete the mission, which is the major difference between the two designs.

The design space between the final designs in cases 4 and 5 was examined by linearly varying the design variables, starting with the case 4 design and ending with the case 5 design. The range and landing angle of attack for designs in between cases 4 and 5 are very poor, as can be seen in Figure 15, and would violate the constraints placed upon our designs. The hump in this curve illustrates how this prevents the optimizer from moving from the case 5 design to the case 4 design. This problem is often encountered, due to the jagged design space, which is caused by noisy analysis routines. This problem is discussed in detail by Giunta *et al.*[20]

A fourth optimization was performed to better explore the design space. This optimization, case 6, started with the design shown in Figure 16 and ended with the design shown in Figure 17. These designs are compared in Table 9.

This design has an unusual wing design and a low wing weight. We discovered this wing weight is unrealistic by performing a finite element structural optimization on the wing planform. The structural optimization indicated

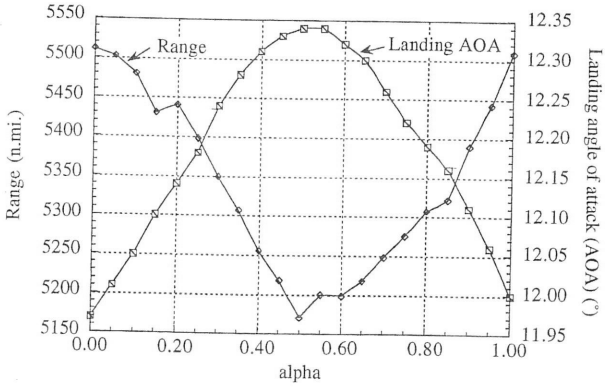

Figure 15. Plot of range and landing angle of attack, for design space between Cases 4 and 5.

the wing weight for this design is significantly higher than what the weight equation calculated. In cases 3 through 6, the majority of the weight increase comes in the form of fuel. This indicates an aerodynamic deficiency, instead of a structural problem. Adding the horizontal tail to the design increases drag, which is costly in terms of weight, but ob-

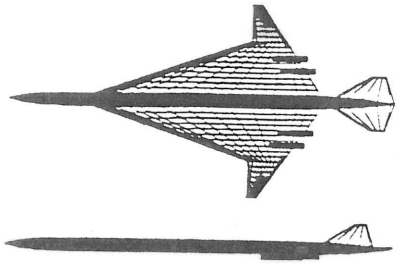

Figure 16. Case 6, initial design

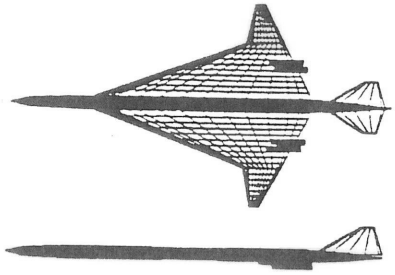

Figure 17. Case 6, final design

Table 9

Comparison of Starting and Ending Designs for Case 6

	Initial	Final	% change
Gross Weight (*lbs*)	583,200	641,500	10.00
Fuel Weight (*lbs*)	281,700	324,400	15.15
Fuel / Gross	48.3%	50.6%	4.76
Wing Area (ft^2)	12,247	12,851	4.93
Wing Weight (*lbs*)	90,200	101,000	11.97
Vert. Tail Area (ft^2)	450.0	720.8	60.18
Vert. Tail Wt (*lbs*)	1,700	2,700	53.61
Horz. Tail Area (ft^2)	1,500.0	1,362.9	-9.14
Horz. Tail Wt (*lbs*)	7,900	7,300	-7.39
Aspect Ratio	2.00	212	6.00
LE Sweep: inboard	70.83°	69.65°	-1.67
outboard	0.00°	12.72°	------
TE Sweep: inboard	65.18°	60.57°	-7.07
outboard	-34.03°	-27.58°	18.95
Nacelle 2 loc., y (*ft*)	35.6	35.5	-0.20
Range (*nm*)	5,081.9	5,504.7	8.42
Landing Angle (°)	12.15	11.92	-1.89
$(L/D)_{max}$	9.352	9.477	1.34

viously the horizontal tail is necessary for the aircraft to take off.

Another source of weight in these designs is the vertical tail, which increased in size for each case. This added not only structural weight, but drag, necessitating the addition of more fuel. In most cases, there was little change in the outboard engine nacelle location, but the vertical tail size increased to allow the engines to safely be located at that position.

Conclusions

We have added essentail trim and control effects to our HSCT design methodology. The variable complexity technique of interlacing the approximate stability derivative predictions with the more accurate VLM predictions worked satisfactorily. Although the derivatives were only updated with the VLM predictions once every 5 optimization cycles, there was good agreement between the approximate predictions and the more accurate predictions.

Adding the engine-out consideration forces the vertical tail to be sized based on the engine location. This resulted in an increase in vertical tail size in cases 1 and 2. Although the weight increased in case 1, the final design meets important requirements that the baseline does not meet.

We found that the spanwise engine location is constrained not by the aerodynamic control requirements, but by the engine strike constraint, which requires the engines do not strike the runway at landing. This is mainly a function of spanwise engine location, main landing gear length and position, and landing attitude. This constraint also affected the inboard trailing edge sweep, reducing it to almost zero to allow the engines to move outboard. Reducing the landing pitch angle also allows the engines to move outboard. This can have a significant effect on the optimized design even for small reductions in landing pitch angle.

The horizontal tail size is based on the requirement that the aircraft must rotate to the take-off position prior to $0.9V_{min}$. The tail size required to do this is highly dependent on the positioning of the landing gear. The tail deflection for approach trim was not critical for any of our designs.

The increased vertical tail size and the addition of a horizontal tail add less than 2.5% to the gross take-off weight, but they result in drag penalties, which translate to large increases in weight. This increased weight is primarily fuel, generally about 75%. The rest of the weight increase is due to the greater amount of fuel being carried, not to structural problems, which would be indicated by changes in the wing planform. Although we found that trim and control increased the weight, adding these considerations provides a more realistic model and better designs.

Acknowledgments

This work was supported by the NASA Langley Research Center under grant NAG1-1160. Peter Coen is the grant monitor. We also wish to acknowledge the support of Arnie McCullers of Vigyan and author of FLOPS for his considerable assistance.

References

1. Hutchison, M.G., Unger, E., Mason, W.H., Grossman, B., and Haftka, R.T., "Variable-Complexity Aerodynamic Optimization of a High Speed Civil Transport Wing," *Journal of Aircraft,* Vol. 31, No. 1, Jan-Feb. 1994, pp. 110-116.
2. Hutchison, M. G., Huang, X., Mason, W. H., Haftka, R. T., and Grossman, B., "Variable-Complexity Aerodynamic-Structural Design of a High-Speed Civil Transport Wing," AIAA Paper 92-4695, Sept. 1992.
3. Hutchison, M. G., Mason, W. H., Grossman, B., and Haftka, R. T., "Aerodynamic Optimization of an HSCT Configuration Using Variable-Complexity Modeling," AIAA Paper 93-0101, Jan. 1993.
4. Kay, J., Mason, W. H., Durham, W., and Lutze, F., "Control Authority Assessment in Aircraft Conceptual Design," AIAA Paper 93-3968, Aug. 1993.
5. McCarty, C.A., Feather, J.B., Dykman, J.R., Page, M.A., and Hodgkinson, J., "Design and Analysis Issues of Integrated Control Systems for High-Speed Civil Transports," NASA CR 186022, May 1992.
6. Sliwa, S.M., "Impact of Longitudinal Flying Qualities Upon the Design of a Transport With Active Controls," AIAA Paper 80-1570, 1980.
7. Sliwa, S.M., "Sensitivity of Optimal Preliminary Design of a Transport to Operational Constraints and Performance Index," AIAA Paper 80-1895, Aug. 1980.
8. Gallman, J.W., Smith, S.C., and Kroo, I.M., "Optimization of Joined-Wing Aircraft," *Journal of Aircraft*, Vol. 30, No. 6, Nov.-Dec. 1993, pp. 897-905.
9. J. Dudley, X. Huang, R.T. Haftka, B. Grossman and W.H. Mason, "Variable-Complexity Interlacing of Weight Equation and Structural Optimization for the Design of the High Speed Civil Transport," AIAA Paper 94-4377, Panama City, Fl., September 1994.
10. FAR Part 25, FAA, Washington, DC.
11 MIL-STD-1797. *Flying Qualities of Piloted Vehicles*, 1987.
12. Roskam, J., *Airplane Design Part V: Component Weight Estimation*, Roskam Aviation and Engineering Corporation, Kansas, 1985.
13. McCullers, L.A., "Aircraft Configuration Optimization Including Optimized Flight Profiles," NASA CP-2327, Proceedings of Symposium on Recent Experiences in Multidisciplinary Analysis and Optimization, J. Sobieski, compiler, April 1984, pp. 396-412.

14. Hoak, D.E., et al, USAF Stability and Control Datcom, Flight Control Division, Air Force Flight Dynamics Laboratory, WPAFB, Ohio, 45433-0000, 1978, revised.
15. Roskam, J. , *Methods for Estimating Stability and Control Derivatives of Conventional Subsonic Airplanes*, Roskam Aviation and Engineering Corporation, Kansas, 1971.
16. Heffley, R. K., and Jewell, W. F., "Aircraft Handling Qualities Data," NASA CR-2144, 1972.
17. Torenbeek, E., *Synthesis of Subsonic Airplane Design*, Delft University Press, 1982, pp. 353.
18. Grandhi, R. V., Thareja, R., and Haftka, R. T., "NEWSUMT-A: A General Purpose Program for Constrained Optimization using Constraint Approximations," *ASME Journal of Mechanisms, Transmissions, and Automation in Design*, 107, pp. 94-99, 1985.
19. Craidon, C.B., "Description of a Digital Computer Program for Airplane Configuration Plots," NASA TM X-2074, 1970.
20. Giunta, A.A., Dudley, J.M., Grossman, B, Haftka, R.T., Mason, W.H., and L.T., Watson, "Noisy Aerodynamic Response and Smooth Approximations in HSCT Design," AIAA Paper 94-4376, Panama City, Fl., September 1994.

Appendix A - Stability Derivative Estimation

We need a fast and simple method to calculate the stability derivatives. The primary use of this method is to predict the trends of the derivatives, as the design of our aircraft changes. Then, these trends are used with a more accurate prediction to update the stability derivatives . To predict the trends, we use the estimation methods from DATCOM.

We assume the vertical tail affects six of the nine stability derivatives: $C_{y\beta}$, $C_{l\beta}$, $C_{n\beta}$, $C_{y\delta r}$, $C_{l\delta r}$, and $C_{n\delta r}$. The other three derivatives, $C_{y\delta a}$, $C_{l\delta a}$, and $C_{n\delta a}$, are assumed to be independent of changes in the vertical tail size. In the case of $C_{y\beta}$, $C_{l\beta}$, and $C_{n\beta}$, only the vertical tail contribution to the stability derivative is calculated, since that is the only contribution that should change with a change in vertical tail size.

The vertical tail contribution for $C_{y\beta}$, is calculated using:

$$C_{y\beta_v} = -kC_{L\alpha_v}\left(1+\frac{d\sigma}{d\beta}\right)\eta_v\frac{S_v}{S} \qquad (A1)$$

where k is an empirical factor defined in Figure A1. The term

$$\left(1+\frac{d\sigma}{d\beta}\right)\eta_v$$

is calculated from:

$$\left(1+\frac{d\sigma}{d\beta}\right)\eta_v = 0.724+3.06\left(\frac{S_v/S}{1+\cos\Lambda_{c/4}}\right)+ 0.4\frac{Z_w}{d}+0.009A \qquad (A2)$$

where Z_w is the vertical distance from the wing root quarter chord point to the fuselage centerline, positive downward.

The vertical tail lift-curve slope is calculated using:

$$C_{L\alpha_v} = \frac{2\pi A_{v_{eff}}}{2+\sqrt{\frac{A_{v_{eff}}^2}{k^2}\left(\beta^2+\tan^2\Lambda_{c/2}\right)+4}} \qquad (A3)$$

with $\beta=\sqrt{1-M^2}$, and where $A_{v_{eff}}$ comes from:

$$A_{v_{eff}} = \left(\frac{A_{v(B)}}{A_v}\right)A_v \qquad (A4)$$

with A_v being the geometric aspect ratio for the isolated vertical tail, $A_{v(B)}/A_v$ is the ratio of the aspect ratio of the vertical panel in the presence of the body to that of the isolated panel, assumed to be 1. This method is only applicable to a singe vertical tail on the plane of symmetry.

The vertical tail contribution to $C_{l\beta_v}$ is given as

$$C_{\ell\beta_v} = C_{y\beta_v}\left(\frac{Z_v\cos\alpha-\ell_v\sin\alpha}{b}\right) \qquad (A5)$$

where and Z_v are the x and z distances, respectively, between the airplane center of gravity and the vertical tail aerodynamic center, see Figure A2.

Similarly, the vertical tail contribution to $C_{n\beta}$ is given as

$$C_{n\beta_v} = -C_{y\beta_v}\left(\frac{\ell_v\cos\alpha+Z_v\sin\alpha}{b}\right) \qquad (A6)$$

The derivative $C_{y\delta r}$ is calculated by:

$$C_{y\delta r} = C_{L\alpha_v}\left[\frac{(\alpha_\delta)_{C_L}}{(\alpha_\delta)_{C_\ell}}\right](\alpha_\delta)_{C_\ell}K'K_b\frac{S_v}{S} \qquad (A7)$$

where

$$\left[\frac{(\alpha_\delta)_{C_L}}{(\alpha_\delta)_{C_\ell}}\right](\alpha_\delta)_{C_\ell}$$

is calculated from Figure A3, and K_b is found using:

$$K_b = \frac{2}{\pi}\left[b_f\sqrt{1-b_f^2}+\sin^{-1}b_f\right] \qquad (A8)$$

As a first approximation, K' was assumed to be 1.

The derivative $C_{l\delta r}$ is found from:

$$C_{\ell\delta r} = C_{y\delta r}\left(\frac{Z_v\cos\alpha-\ell_v\sin\alpha}{b}\right) \qquad (A9)$$

Similarly, $C_{n\delta r}$ is found from:

$$C_{n\delta r} = C_{y\delta r}\left(\frac{\ell_v\cos\alpha+Z_v\sin\alpha}{b}\right) \qquad (A10)$$

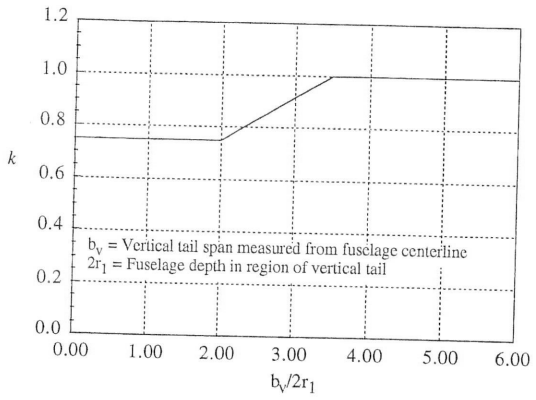

Figure A1

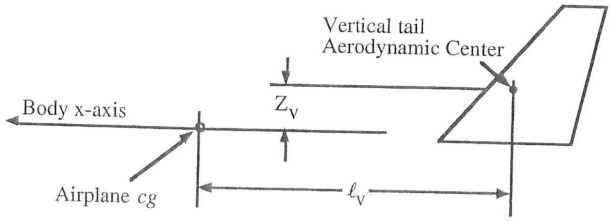

Figure A2

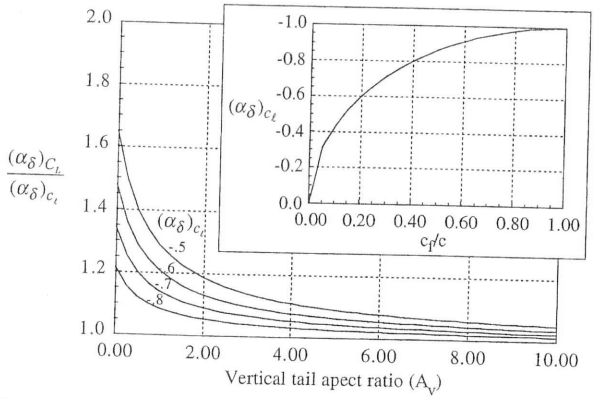

Figure A3